

Conjugated Extension of Non-Fullerene Acceptors Enables Efficient Organic Solar Cells with Optoelectronic Response over 1000 nm

Bailin Zhou,[†] Yalu Zou,[†] Yuan-Qiu-Qiang Yi, Zhixiang Li, Guankui Long, Yang Yang, Jian Wang, Xiangjian Wan, Chenxi Li, Zhaoyang Yao,* and Yongsheng Chen*



Cite This: *ACS Appl. Energy Mater.* 2022, 5, 4664–4672



Read Online

ACCESS |



Metrics & More



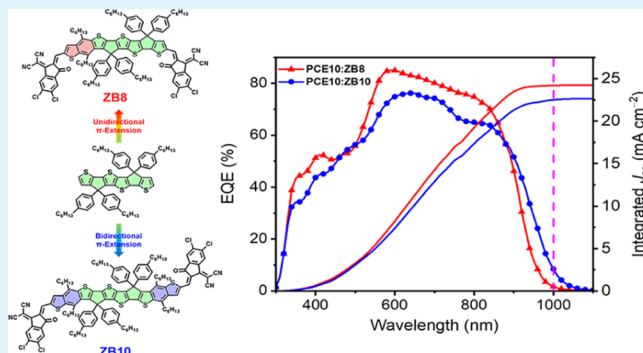
Article Recommendations



Supporting Information

ABSTRACT: The efficient near-infrared response of light-active materials is one of the prerequisites for the most advanced organic solar cells (OSCs). Two benzodithiophene fused-ring cores (BT-4T and DBT-4T), featured with stepwise enlarged conjugations and improved electron-donor characteristics, are designed and used as the central donor units for the construction of acceptor–donor–acceptor-type molecules ZB8 and ZB10. The significantly enhanced intramolecular charge transfer endows ZB8- and ZB10-based OSCs with a photoelectronic response over 1000 nm. With more favorable molecular energy levels and an asymmetric configuration, ZB8-based best OSCs afford a 12.30% power conversion efficiency, better than that of 11.08% for the ZB10-based one. Our successful exploration for electron-rich fused-ring cores provides a quite rare but promising platform for highly efficient OSCs with a photoelectronic response over 1000 nm.

KEYWORDS: organic solar cells, acceptor–donor–acceptor molecules, near-infrared materials, fused-ring cores, asymmetric configuration



1. INTRODUCTION

Organic solar cells (OSCs) have drawn significant attention as a clean renewable energy technology in the past decades because of their lightweight, mechanical flexibility, and solution processability.^{1–8} Thanks to the rapid development of active layer molecules and device optimization, especially for the extensive exploration for non-fullerene acceptors (NFAs), OSCs have approached an excellent PCE of 19% with the highly strong absorption limiting to ~930 nm.^{9–17} The remaining huge efficiency gap of PCEs between OSCs and commercially available silicon solar cells, which possess a photon response close to 1100 nm, could be partially attributed to the insufficient absorptions within 900–1100 nm for state-of-the-art OSCs. This can be further modeled by our semi-empirical analysis,¹⁸ that is, over 20% PCEs can be achieved if the range of absorption onset is 900–1100 nm for a single-junction OSC on the basis of the average external quantum efficiency (EQE) of 80%, energy loss (E_{loss}) below 0.45 eV, and fill factor (FF) of 80%. Therefore, the exploration for near-infrared (NIR) materials is becoming more and more urgent and has drawn extensive scientific attention in light of their desirable applications in tandem, ternary, semitransparent OSCs and even some other devices like NIR photodetectors and so on.^{19–26} However, thus far, very few systems with both high efficiency and a broad photoelectronic response over 1000 nm have been developed, mainly due to the great challenges of

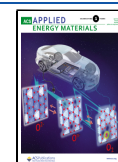
feasible construction of electron-donating cores and delicately tuning energy levels of NFAs.

Typical NFAs, which play a dominant role in harvesting low-energy photons for OSCs, are usually featured with an architecture of acceptor–donor–acceptor (A–D–A).^{27–29} The inherited unique frontier molecular orbital distributions from the A–D–A-type structure contribute to the distinctive merits of conveniently tunable band gaps and energy levels, more importantly, exceptional exciton separation and carrier transport features.^{30–38} In the framework of A–D–A structures, increasing the electron-donating capacity of central backbones and/or the electron-withdrawing capacity of end groups to enhance the intramolecular charge transfer (ICT) has been regarded as the most effective strategy to develop NIR NFAs.^{39–42} Among them, the conjugated extension of linear backbones of central donors could increase the electron-donating ability to result in NFAs significantly, in favor of a highly strong ICT and thus a reduced optical band gap.^{43–47} Moreover, the unidirectional extension of backbones usually results in NFAs with asymmetric configurations, leading to

Received: January 8, 2022

Accepted: March 9, 2022

Published: March 22, 2022



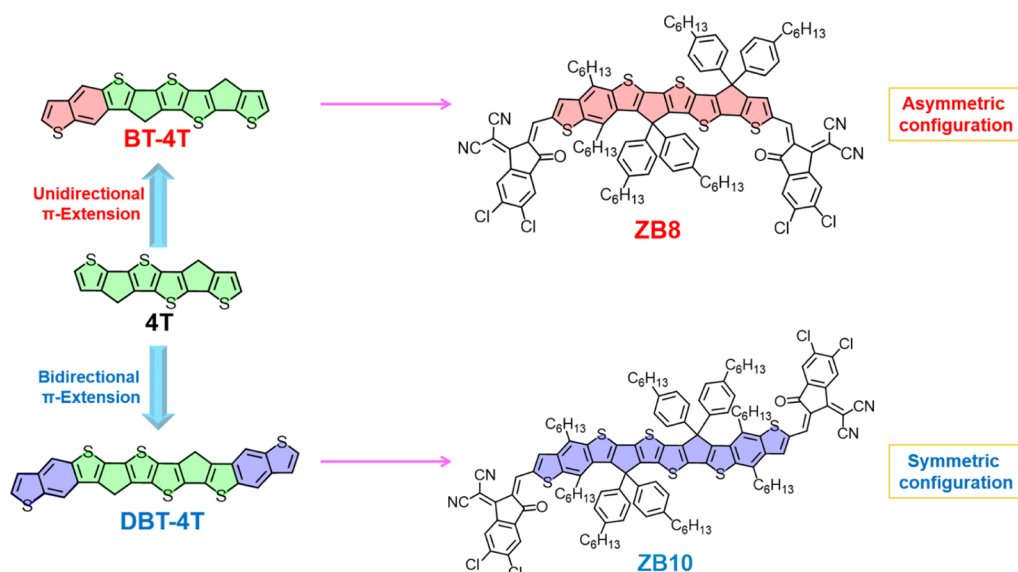
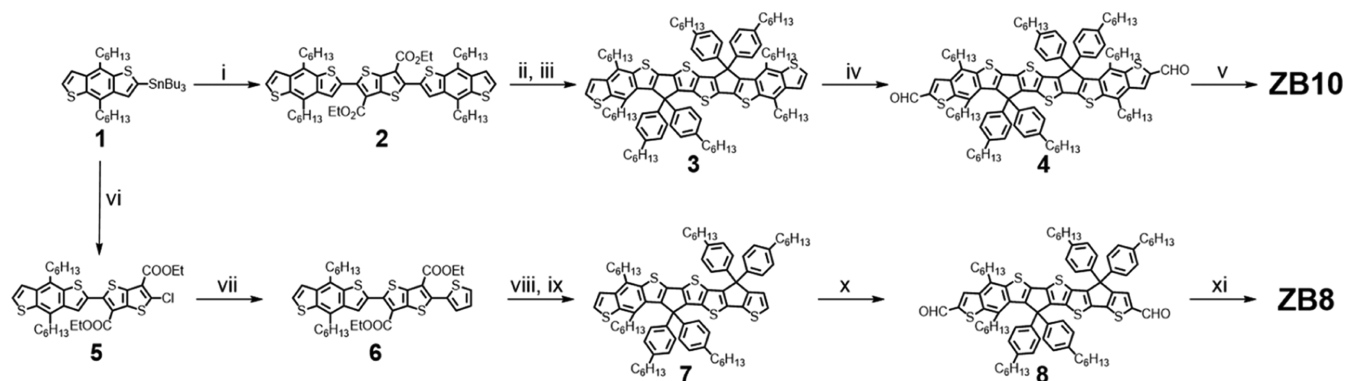


Figure 1. Construction of donor cores (BT-4T and DBT-4T) by uni- or bidirectional conjugated extension of 4T and chemical structures of ZB8 and ZB10.

Scheme 1. Synthetic Routes of ZB8 and ZB10^a



^aReagents and conditions: (i) 2,5-dichlorothiopheno[3,2-*b*]thiophene-3,6-dicarboxylate, Pd(PPh₃)₄, toluene, 110 °C, overnight; (ii) (4-hexylphenyl)lithium, THF, −78 °C to rt, overnight; (iii) Amberlyst 15, toluene, 80 °C, overnight; (iv) DMF, POCl₃, DCE, 80 °C, overnight; (v) IC-2Cl, pyridine, chloroform, rt, overnight; (vi) 2,5-dichlorothiopheno[3,2-*b*]thiophene-3,6-dicarboxylate, Pd(PPh₃)₄, toluene, 110 °C, overnight; (vii) tributyl(thiophen-2-yl)stannane, Pd(PPh₃)₄, toluene, 110 °C, overnight; (viii) (4-hexylphenyl)lithium, THF, −78 °C to rt, overnight; (ix) Amberlyst 15, toluene, 80 °C, overnight; (x) DMF, POCl₃, DCE, 80 °C, overnight; (xi) IC-2Cl, pyridine, chloroform, rt, overnight.

enlarged dipole moments and further increased intermolecular binding energies.^{33,48} For the acceptor parts, IC-2Cl⁴⁹ has been proven to possess a very strong electron-withdrawing ability, which is conducive to achieving NIR NFAs. Chlorination at end groups can downshift the molecular energy levels effectively, especially for the LUMOs.

Bearing the above discussions in mind, we synthesized two benzodithiophene fused-ring cores, BT-4T and DBT-4T (Figure 1), through uni- or bidirectional π -extension of the central donor (4T) reported by our previous work.⁵⁰ Then, capping the strong electron-withdrawing end groups of IC-2Cl to central donors affords two A–D–A-type NFAs, ZB8 and ZB10 (Figure 1). The improved electron-donating property of central donor units enhances the ICT significantly, endowing ZB8 and ZB10 with strong NIR absorptions. Note that OSCs based on ZB8 and ZB10 exhibited a photoelectronic response over 1000 nm, making them among very few systems with such a broad absorption and high efficiency. Moreover, due to the more favorable molecular energy levels and asymmetric

configuration, ZB8-based OSCs render a superior PCE of 12.30% with respect to that of 11.08% for the ZB10-based one, accompanied by an excellent V_{oc} of 0.702 V, a J_{sc} of 25.77 mA cm^{−2}, and an FF of 68.01%. These results demonstrate that the constructed BT-4T and DBT-4T donor cores exhibit a promising prospect for the development of NIR NFAs and provide a quite rare but promising platform for efficient OSCs with a photoelectronic response over 1000 nm.

2. RESULTS AND DISCUSSION

2.1. Synthesis and Characterization.

In Scheme 1, the starting compound 1 was applied by the Stille coupling with 1 or 0.5 equiv 2,5-dichlorothiopheno[3,2-*b*]thiophene-3,6-dicarboxylate to generate compounds 5 and 2 in moderate yields, respectively. Then, compound 5 was further followed by another Stille coupling with tributyl(thiophen-2-yl)stannane to yield intermediate 6. Later, 2 and 6 were implemented in a carbonyl addition reaction with (4-hexylphenyl)lithium to afford tertiary alcohols, which were not isolated and

subsequently underwent intramolecular Friedel–Crafts cyclization catalyzed by Amberlyst 15 to produce the central donors of **3** and **7**. Due to the highly strong electron-rich property, both **3** and **7** were sensitive to air and easily decomposed on the silica gel columns. Therefore, without purification, compounds **3** and **7** were directly transformed into the corresponding dialdehydes through the Vilsmeier–Haack reaction. Finally, target NFAs **ZB8** and **ZB10** were afforded with decent yields via a condensation reaction between the above dialdehydes and IC-2Cl. The definite synthetic methods and characterizations are depicted in the Supporting Information.

2.2. Theoretical Calculations. We performed the density functional theory (DFT) calculations^{51,52} to evaluate the frontier molecular orbitals, molecular geometries, and dipole moments of **ZB8** and **ZB10**. As displayed in Figure 2, both

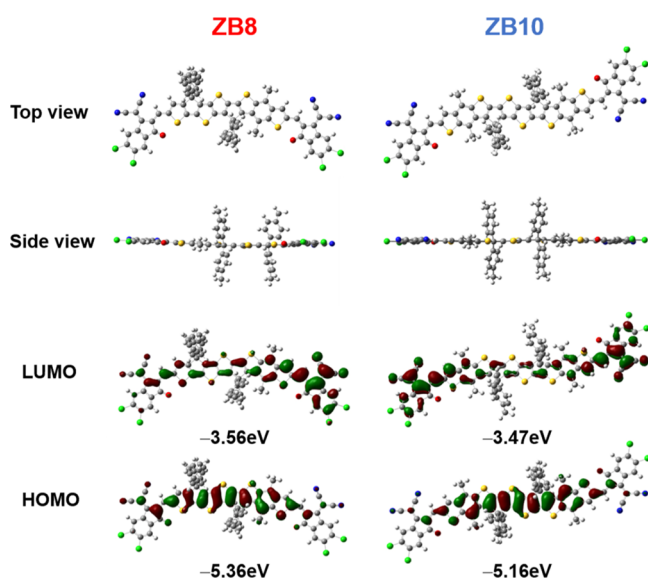


Figure 2. Optimized molecular geometries and calculated energy levels of **ZB8** and **ZB10**. The large aliphatic groups were substituted with methyl to simplify the computation. The involved LUMO and HOMO energy levels are given for a quantitative comparison.

ZB8 and **ZB10** possess a rather planar backbone, which is conducive to enhancing the ICT and intermolecular π – π stacking. As it is expected, the LUMOs are located mainly on the end groups of IC-2Cl, while the HOMOs are primarily distributed along the backbones of the central donors. This feature is widely observed for the A–D–A-type molecules, leading to an enhanced molar extinction coefficient and a better exciton separation and carrier transport.³⁸ The calculated LUMOs and HOMOs of **ZB8** and **ZB10** are $-3.56/-5.36$ eV and $-3.47/-5.16$ eV, respectively. The obviously upshifted HOMO of **ZB10** with respect to that of **ZB8** should be attributed to its more extensive conjugated extension of the central donor. In addition, the dipole moments of **ZB8** and **ZB10** were also calculated (Figure S1), showing 2.21 D and 15.20 D for the ground and excited states of **ZB8** and both 0 D for those of **ZB10**. The much larger dipole moments of **ZB8** should be attributed to its asymmetric molecular configuration caused by the unidirectional π -extension.^{53,54} Therefore, the significant dipole–dipole interaction of **ZB8** is expected to induce more intensive packing of adjacent molecules, in favor of an efficient charge

transport and thus an improved FF of OSCs.^{55–57} The detailed parameters are presented in Table S1.

2.3. Optical and Electrochemical Properties. The UV–vis absorption spectra of **ZB8** and **ZB10** in solutions and solid films are shown in Figure 3a,b. **ZB10** possesses the maximum absorption peak at 802 nm in solution, shifted by nearly 10 nm compared to that of 791 nm for **ZB8**, which should be ascribed to the longer conjugated framework of **ZB10**. The maximum molar extinction coefficient of **ZB8** is $1.64 \times 10^5 \text{ M}^{-1} \text{ cm}^{-1}$, larger than that of $1.22 \times 10^5 \text{ M}^{-1} \text{ cm}^{-1}$ for **ZB10**. Note that ~ 55 nm red-shifted maximum absorption peaks can be observed from solutions to solid films for both **ZB8** and **ZB10**, suggesting the strong intermolecular interactions.^{58,59} The film absorption onsets of **ZB8** and **ZB10** are 946 and 990 nm, with corresponding band gaps of 1.31 and 1.25 eV, displaying strong absorption in the NIR region. The frontier molecular orbital energy levels are shown in Figure 3c, gauged by cyclic voltammetry (CV) measurements (Figure S2). The LUMOs/HOMOs of **ZB8** and **ZB10** were determined to be $-4.08/-5.59$ and $-4.03/-5.43$ eV, respectively, with the band gaps of 1.51 and 1.40 eV. Note that the relative alignment of energy levels matches well with the calculated data from DFT calculations. Obviously, the conjugated extension of the central donor contributes to the much higher HOMO energy level and strong NIR absorption of **ZB10** with respect to that of **ZB8**. The detailed data of physicochemical properties of **ZB8** and **ZB10** are listed in Table 1.

2.4. Photovoltaic Performance of OSCs. As shown in Figure 3b,c, the polymeric donor of PCE10⁶⁰ matches well with **ZB8** and **ZB10** in terms of both absorption and energy levels. Therefore, an inverted OSC with the structure of ITO/ZnO/PFN-Br/PCE10:acceptor/MoO₃/Ag (Figure 3d) was fabricated. The detailed data of device optimization are listed in Tables S2–S7, and the photovoltaic parameters of champion OSCs are shown in Figure 3e,f and Table 2. PCE10:**ZB10**-based OSCs show a relatively high V_{oc} (0.734 V) and a moderate J_{sc} (24.05 mA cm⁻²) and FF (62.75%), affording a PCE of 11.08%. On the contrary, the champion OSC based on PCE10:**ZB8** affords a trifle lower V_{oc} of 0.702 V but a much increased J_{sc} (25.77 mA cm⁻²) and FF (68.01%), giving rise to a better PCE of 12.30% with respect to that of PCE10:**ZB10**. The relatively lower V_{oc} for **ZB8**-based OSCs agrees with the down-shifted LUMO of **ZB8** compared to that of **ZB10**. As displayed in Table S8, the total energy losses (E_{loss}) of **ZB8**- and **ZB10**-based OSCs have been calculated, being 0.636 and 0.562 eV, respectively. Moreover, the non-radiative recombination losses (ΔE_3) of **ZB8**- and **ZB10**-based OSCs are 0.326 and 0.262 eV, respectively. Although the smaller E_{loss} is conducive to a higher V_{oc} for **ZB10**-based OSCs, the much lower J_{sc} and FF render an inferior PCE with respect to that of **ZB8**-based devices. The detailed calculation method of E_{loss} is represented in the Supporting Information and shown in Figures S3 and S4. Note that the EQE spectrum of OSCs employing PCE10:**ZB10** as the active layer features a markedly broader photoelectric response range even over 1000 nm (Figure 3f). However, unfortunately, the EQE values of PCE10:**ZB10** devices generally are much lower compared to that of PCE10:**ZB8**-based OSCs, which should correspond to the inferior J_{sc} of **ZB10**-based OSCs. The higher EQE for **ZB8**-based OSCs in the extent of 500–900 nm should be attributed to the combined factors of a much stronger light absorption with respect to that of the **ZB10**-based one (Figure S5), the superior efficiency of exciton dissociation driven by the

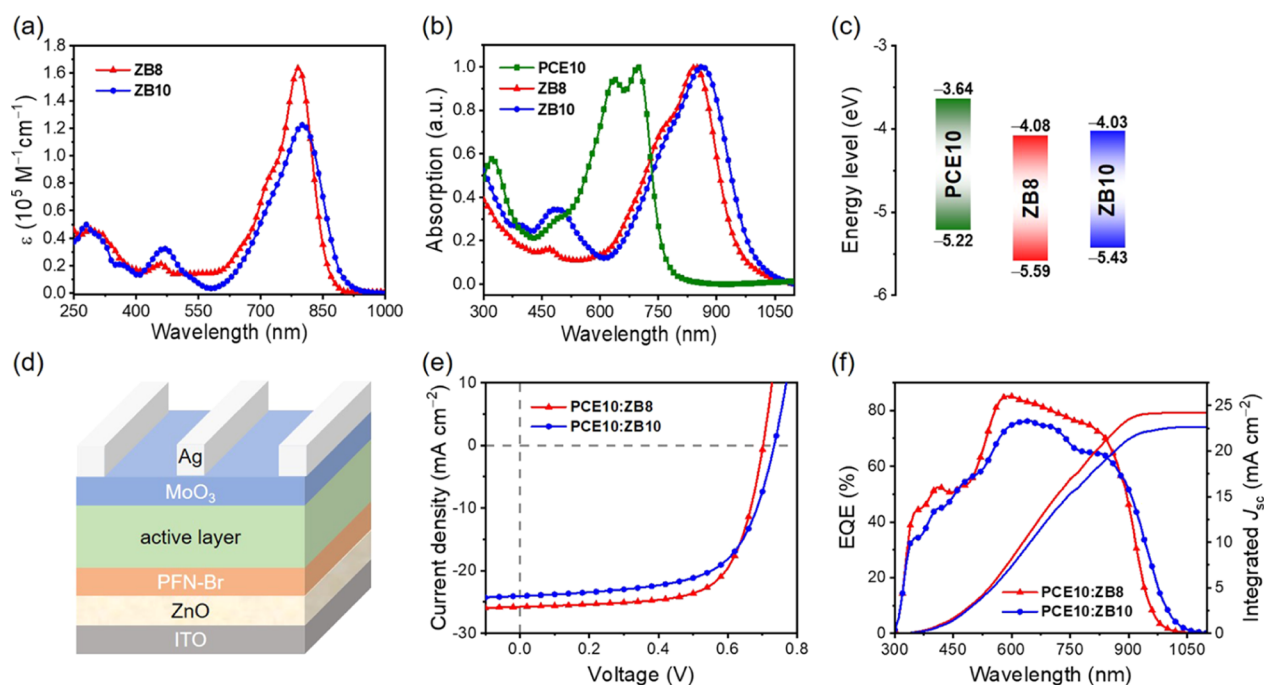


Figure 3. (a) Electron absorption spectra of **ZB8** and **ZB10** dissolved in diluted chloroform (10^{-6} M). (b) Normalized electron absorption spectra of **PCE10**, **ZB8**, and **ZB10** thin films. (c) Energy level diagrams of **PCE10**, **ZB8**, and **ZB10** derived from the corresponding CVs. (d) Device architecture. (e) J - V curves and (f) EQE curves of **PCE10:ZB8**- and **PCE10:ZB10**-based OSCs.

Table 1. Physicochemical Properties of ZB8 and ZB10

NFAs	$\lambda_{\max}^{\text{CF}}$ (nm)	$\lambda_{\max}^{\text{film}}$ (nm)	$\lambda_{\text{edge}}^{\text{film}}$ (nm)	HOMO (eV)	LUMO (eV)	E_{g}^{CV} (eV)	$E_{\text{g}}^{\text{opt}}$ (eV)
ZB8	791	845	946	-5.59	-4.08	1.51	1.31
ZB10	802	863	990	-5.43	-4.03	1.40	1.25

significantly enlarged HOMO energy offset between **PCE10** and **ZB8**, and the more efficient charge collection discussed below. In addition, the improved FF for **ZB8**-based OSCs with respect to that of the **ZB10**-based one might be caused by **ZB8**'s both increased hole and electron mobilities and more balanced ratio discussed below. Note that the integrated J_{sc} of the optimized OSCs is in good accordance with that derived from J - V curves, with an error of less than 5%.

2.5. Device Characterization. As shown in Figure 4a, we measured the correlation between photocurrent densities (J_{ph}) and effective voltages (V_{eff}) for optimized OSCs.^{61,62} Both OSCs reach their saturated current densities (J_{sat}) when V_{eff} is nearly 1.5 V, indicating that the OSCs have negligible charge recombination under high voltages.⁶³ The derived exciton dissociation efficiency (P_{diss}) and carrier collection efficiency (P_{coll}) are 93.5%/76.8% and 91.0%/72.1% for **ZB8**- and **ZB10**-based OSCs, respectively, which should partially account for the improved EQE and J_{sc} for **ZB8**. Note that the higher P_{diss} for the **ZB8**-based device is caused by its downshifted HOMO, giving rise to the more efficient exciton dissociation with a larger driving force. The charge recombination mechanism was

also analyzed by measuring the J_{sc} and V_{oc} characteristics of **ZB8**- and **ZB10**-based OSCs under different light densities (P). J_{sc} and P follow $J_{\text{sc}} \propto P^{\alpha}$, where α can indicate whether the OSCs have a severe bimolecular recombination.⁶⁴ In Figure 4b, the α of **ZB8**- and **ZB10**-based OSCs are 0.96 and 0.95, implying that both OSCs have a negligible bimolecular recombination. Besides, the relationship between V_{oc} and P is followed by $V_{\text{oc}} \propto S \ln P$, where the slope, S , indicates the extent of a trap-assisted recombination. When S is close to $2kT/q$, it means that the trap-assisted recombination is severe. The trap-free charge transport can be indicated by the S value closer to kT/q .⁶⁵ As shown in Figure 4c, the values of S for **ZB8**- and **ZB10**-based OSCs are $1.26kT/q$ and $1.32kT/q$, suggesting both weak but slightly reduced trap-assisted recombination for **ZB8**-based OSCs with respect to that of the **ZB10**-based one.

To shed light on the improved J_{sc} and FF for **ZB8**-based OSCs, the charge mobilities were measured and are shown in Figure S6 and diagrammed in Figure 4d. The electron (μ_{e}) and hole mobilities (μ_{h}) of **ZB8**- and **ZB10**-based OSCs can be calculated to be $5.6 \times 10^{-4}/6.34 \times 10^{-4}$ and $3.5 \times 10^{-4}/5.07 \times 10^{-4} \text{ cm}^2 \text{ V}^{-1} \text{ s}^{-1}$, respectively, providing a more balanced ratio of $\mu_{\text{h}}/\mu_{\text{e}}$ (1.13) for **ZB8**-based OSCs compared to that of the **ZB10**-based ones (1.41). The high and balanced carrier mobility is advantageous to carrier transport and suppressed bimolecular recombination,⁶⁶ accounting for the higher J_{sc} and FF for **ZB8**-based OSCs. The enlarged charge mobilities of **PCE10:ZB8** blends may be caused by the significant dipole-

Table 2. Optimized Photovoltaic Parameters of ZB8 and ZB10 (Measured under AM 1.5G, 100 mW cm^{-2})

devices	V_{oc} (V)	J_{sc} (mA cm^{-2})	$J_{\text{sc}}^{\text{EQE}}$ (mA cm^{-2})	FF (%)	PCE^a (%)
PCE10:ZB8	0.702 (0.697 \pm 0.005)	25.77 (25.84 \pm 0.25)	24.53	68.01 (67.11 \pm 0.90)	12.30 (12.09 \pm 0.21)
PCE10:ZB10	0.734 (0.733 \pm 0.007)	24.05 (23.80 \pm 0.46)	22.93	62.75 (62.42 \pm 1.43)	11.08 (10.90 \pm 0.18)

^aThe average parameters included in the brackets were calculated from more than 20 devices.

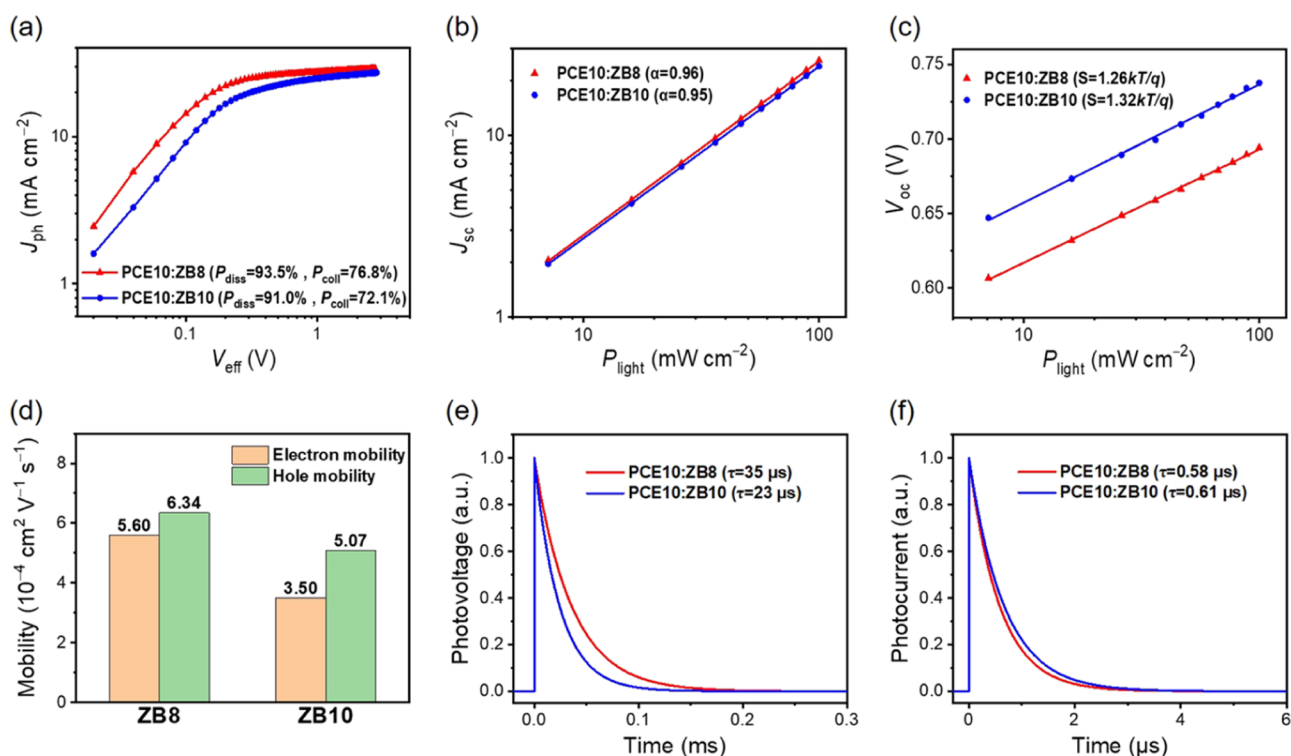


Figure 4. (a) Plots of J_{ph} vs V_{eff} for ZB8- and ZB10-based OSCs. (b) J_{sc} characteristics of ZB8- and ZB10-based OSCs under different light densities, where a negligible bimolecular recombination can be achieved if α gets close to 1. (c) V_{oc} characteristics of ZB8- and ZB10-based OSCs under different light densities, where the trap-free charge transport can be indicated by the S value getting close to kT/q . (d) Charge mobilities' histogram. (e) TPV and (f) TPC of ZB8- and ZB10-based OSCs.

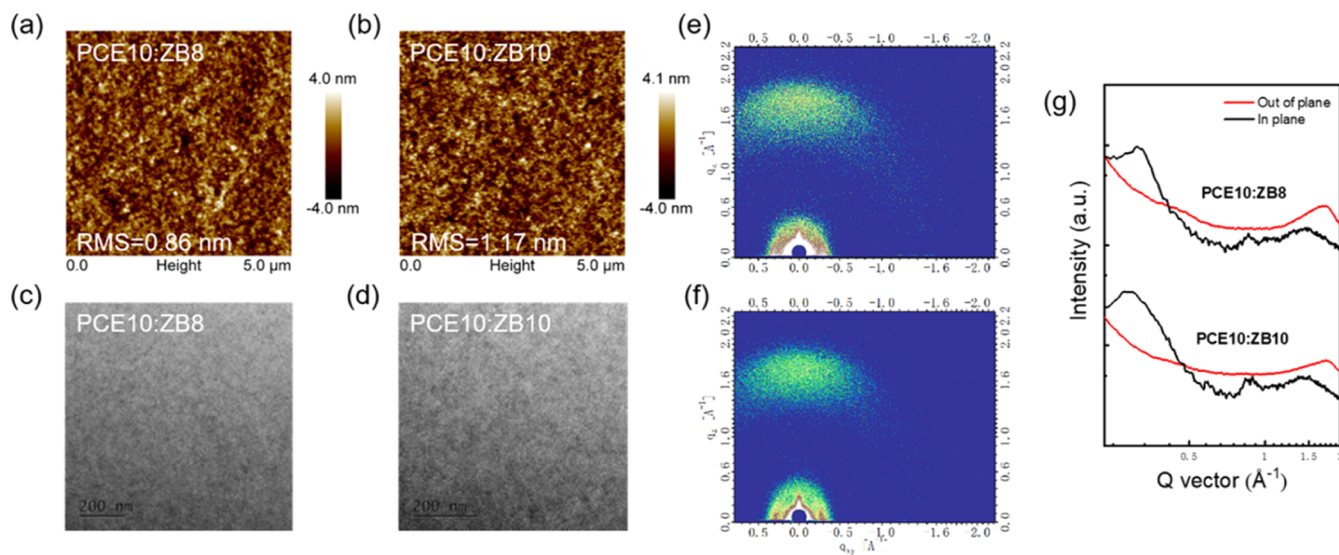


Figure 5. AFM pictures for (a) PCE10:ZB8 and (b) PCE10:ZB10 blends. TEM pictures for (c) PCE10:ZB8 and (d) PCE10:ZB10 blends and (e) 2D-GIWAXS of (e) PCE10:ZB8 and (f) PCE10:ZB10 blends and (g) the corresponding line-cut profiles.

dipole intermolecular actions induced by the asymmetric molecular configuration of ZB8.⁵⁷ To further quantify the carrier recombination and transport processes, transient photovoltage (TPV) and transient photocurrent (TPC) measurements were implemented. As shown in Figure 4e, the charge-carrier lifetime τ can be extracted as 35 and 23 μs for ZB8- and ZB10-based devices, respectively. The prolonged lifetime of ZB8-based OSCs aligns well with their slightly suppressed charge recombination in comparison with that of ZB10.²⁰ Moreover, a little faster charge-extraction process can

be observed for ZB8 with a lifetime of 0.58 μs with respect to that of 0.61 μs for ZB10-based devices (Figure 4f), suggesting a more efficient charge transport in PCE10:ZB8-based OSCs and being in accordance with their higher charge mobilities and thus a better FF.

2.6. Morphology Analysis. We used atomic force microscopy (AFM) and transmission electron microscopy (TEM) to investigate the morphologies of ZB8- and ZB10-based OSCs at the nanoscale. In Figure 5a,b, both blend films of PCE10:ZB8 and PCE10:ZB10 are smooth with root-mean-

square (RMS) roughness values of 0.86 and 1.17 nm, respectively, benefiting effective contact between the light absorption layer and the counter electrode. For the TEM images in Figure 5c,d, the relatively homogeneous morphology and proper domain size can be observed for both blends of PCE10:ZB8 and PCE10:ZB10, in agreement with their both relatively high PCEs. Grazing-incidence wide-angle X-ray scattering (GIWAXS) has been used to unveil the microscopic topography in both neat and blended films based on ZB8 and ZB10. The detailed GIWAXS data are shown in Figure S7 and Table S9. Both ZB8 and ZB10 neat films have small π - π stacking distances (3.53 Å), and they show an obvious face-on orientation. However, the lamellar packing distance of ZB8 (19.32 Å) is smaller than that of ZB10 (21.09 Å), which might be induced by the dipole interactions.⁵⁶ As for PCE10:ZB8 and PCE10:ZB10 blend films (Figure 5e-g), both the intense stackings can be achieved along with the π - π distances of 3.61 and 3.55 Å, respectively. The crystal coherence length corresponding to the (010) diffraction peaks for ZB8- and ZB10-based blend films are also very similar, namely, 12.39 Å and 12.96 Å, respectively. It is noted that the lamellar packing distance of the ZB8-based blend (19.86 Å) is much smaller than that of the ZB10-based one (22.65 Å), which agrees with that of neat films. The suitable intermolecular π - π stacking strength and significantly enhanced lamellar packing of ZB8 may provide an optimized morphology for the ZB8-based blend, further resulting in a better performance of OSCs.⁵⁵

3. CONCLUSIONS

Two A-D-A-type NFAs, ZB8 and ZB10, with an extensive π -extension of the central donor units were synthesized with a high photoelectronic response in the NIR range, making them among very few systems with such a broad EQE spectrum and high efficiency. The unidirectional π -extension of the central donor in ZB8 leads to more favorable molecular energy levels and an asymmetric configuration compared to that of ZB10. As a consequence, the best OSC based on ZB8 affords a superior PCE of 12.30% compared to that of 11.08% for the ZB10-based one, accompanied by an excellent J_{sc} of 25.77 mA cm⁻², an FF of 68.01%, and a V_{oc} of 0.702 V. Our work provides a quite rare but promising platform for highly efficient OSCs with a photoelectronic response over 1000 nm and will stimulate further exploration for NIR materials, which are quite essential for breaking through the PCE bottleneck of OSCs currently.

■ ASSOCIATED CONTENT

SI Supporting Information

The Supporting Information is available free of charge at <https://pubs.acs.org/doi/10.1021/acsaem.2c00092>.

Description of the experimental measurements and instruments; molecular synthesis and characterization; device fabrication and optimization conditions; the calculation method of energy loss; dipole moments of ZB8 and ZB10; cyclic voltammetry plots of ZB8 and ZB10 films; normalized absorption and PL spectra of ZB8 and ZB10 neat films; EQE_{EL} of the devices based on PCE10:ZB8 and PCE10:ZB10; UV-vis absorption spectra of the blend films of PCE10:ZB8 and PCE10:ZB10; electron and hole mobilities of optimized devices; 2D GIWAXS patterns and scattering profiles for

ZB8 and ZB10 neat films; and NMR and HR-MS spectra (PDF)

■ AUTHOR INFORMATION

Corresponding Authors

Zhaoyang Yao – The Centre of Nanoscale Science and Technology and Key Laboratory of Functional Polymer Materials, Institute of Polymer Chemistry, State Key Laboratory of Elemento-Organic Chemistry, College of Chemistry, Renewable Energy Conversion and Storage Center (RECAST), Nankai University, Tianjin 300071, China; orcid.org/0000-0003-1384-183X; Email: zyao@nankai.edu.cn

Yongsheng Chen – The Centre of Nanoscale Science and Technology and Key Laboratory of Functional Polymer Materials, Institute of Polymer Chemistry, State Key Laboratory of Elemento-Organic Chemistry, College of Chemistry, Renewable Energy Conversion and Storage Center (RECAST), Nankai University, Tianjin 300071, China; orcid.org/0000-0003-1448-8177; Email: yschen99@nankai.edu.cn

Authors

Bailin Zhou – The Centre of Nanoscale Science and Technology and Key Laboratory of Functional Polymer Materials, Institute of Polymer Chemistry, State Key Laboratory of Elemento-Organic Chemistry, College of Chemistry, Renewable Energy Conversion and Storage Center (RECAST), Nankai University, Tianjin 300071, China

Yalu Zou – The Centre of Nanoscale Science and Technology and Key Laboratory of Functional Polymer Materials, Institute of Polymer Chemistry, State Key Laboratory of Elemento-Organic Chemistry, College of Chemistry, Renewable Energy Conversion and Storage Center (RECAST), Nankai University, Tianjin 300071, China

Yuan-Qiu-Qiang Yi – Printable Electronics Research Center, Nano Devices and Materials Division, Suzhou Institute of Nano-Tech and Nano-Bionics, Chinese Academy of Sciences, Suzhou 215123 Jiangsu, China; orcid.org/0000-0003-3522-7056

Zhixiang Li – The Centre of Nanoscale Science and Technology and Key Laboratory of Functional Polymer Materials, Institute of Polymer Chemistry, State Key Laboratory of Elemento-Organic Chemistry, College of Chemistry, Renewable Energy Conversion and Storage Center (RECAST), Nankai University, Tianjin 300071, China

Guankui Long – School of Materials Science and Engineering, National Institute for Advanced Materials, Renewable Energy Conversion and Storage Center (RECAST), Nankai University, 300350 Tianjin, China; orcid.org/0000-0002-1826-3736

Yang Yang – The Institute of Seawater Desalination and Multipurpose Utilization, Ministry of Natural Resources (Tianjin), Tianjin 300192, China; orcid.org/0000-0001-9335-8834

Jian Wang – The Institute of Seawater Desalination and Multipurpose Utilization, Ministry of Natural Resources (Tianjin), Tianjin 300192, China

Xiangjian Wan – The Centre of Nanoscale Science and Technology and Key Laboratory of Functional Polymer Materials, Institute of Polymer Chemistry, State Key Laboratory of Elemento-Organic Chemistry, College of Chemistry, Renewable Energy Conversion and Storage Center

(RECAST), Nankai University, Tianjin 300071, China;

orcid.org/0000-0001-5266-8510

Chenxi Li – The Centre of Nanoscale Science and Technology and Key Laboratory of Functional Polymer Materials, Institute of Polymer Chemistry, State Key Laboratory of Elemento-Organic Chemistry, College of Chemistry, Renewable Energy Conversion and Storage Center (RECAST), Nankai University, Tianjin 300071, China

Complete contact information is available at:

<https://pubs.acs.org/10.1021/acsaem.2c00092>

Author Contributions

¹B.Z. and Y.Z. contributed equally to this paper.

Notes

The authors declare no competing financial interest.

ACKNOWLEDGMENTS

The authors gratefully acknowledge the financial support from NSFC (21935007, 52025033, and 51873089) and MoST (2019YFA0705900) of China, Tianjin city (20JCZDJC00740) and 111 Project (B12015).

REFERENCES

- (1) Li, W.; Abd-Ellah, M.; Liu, H.; Li, X.; Yin, Z.; Kumar, P.; Wang, J.; Li, Y. Novel Wide Bandgap Benzodithiophene-Based Polymer Donors with Electron-Withdrawing Indolin-2-One Side Chains for Efficient Organic Solar Cells with High Open Circuit Voltage. *Dyes Pigm.* **2022**, *197*, 109876.
- (2) Lin, Y.; Wang, J.; Zhang, Z.-G.; Bai, H.; Li, Y.; Zhu, D.; Zhan, X. An Electron Acceptor Challenging Fullerenes for Efficient Polymer Solar Cells. *Adv. Mater.* **2015**, *27*, 1170–1174.
- (3) Sun, Y.; Chang, M.; Meng, L.; Wan, X.; Gao, H.; Zhang, Y.; Zhao, K.; Sun, Z.; Li, C.; Liu, S.; Wang, H.; Liang, J.; Chen, Y. Flexible Organic Photovoltaics Based on Water-Processed Silver Nanowire Electrodes. *Nat. Electron.* **2019**, *2*, 513–520.
- (4) Yang, C.; Zhang, S.; Ren, J.; Gao, M.; Bi, P.; Ye, L.; Hou, J. Molecular Design of a Non-Fullerene Acceptor Enables a P3ht-Based Organic Solar Cell with 9.46% Efficiency. *Energy Environ. Sci.* **2020**, *13*, 2864–2869.
- (5) Yuan, J.; Zhang, Y.; Zhou, L.; Zhang, G.; Yip, H.-L.; Lau, T.-K.; Lu, X.; Zhu, C.; Peng, H.; Johnson, P. A.; Leclerc, M.; Cao, Y.; Ulanski, J.; Li, Y.; Zou, Y. Single-Junction Organic Solar Cell with over 15% Efficiency Using Fused-Ring Acceptor with Electron-Deficient Core. *Joule* **2019**, *3*, 1140–1151.
- (6) Zhang, G.; Zhao, J.; Chow, P. C. Y.; Jiang, K.; Zhang, J.; Zhu, Z.; Zhang, J.; Huang, F.; Yan, H. Nonfullerene Acceptor Molecules for Bulk Heterojunction Organic Solar Cells. *Chem. Rev.* **2018**, *118*, 3447–3507.
- (7) Liu, Y.; Liu, B.; Ma, C.-Q.; Huang, F.; Feng, G.; Chen, H.; Hou, J.; Yan, L.; Wei, Q.; Luo, Q.; Bao, Q.; Ma, W.; Liu, W.; Li, W.; Wan, X.; Hu, X.; Han, Y.; Li, Y.; Zhou, Y.; Zou, Y.; Chen, Y.; Li, Y.; Chen, Y.; Tang, Z.; Hu, Z.; Zhang, Z.-G.; Bo, Z. Recent Progress in Organic Solar Cells (Part I Material Science). *Sci. China Chem.* **2021**, *65*, 224–268.
- (8) Feng, S.; Zhang, C. e.; Liu, Y.; Bi, Z.; Zhang, Z.; Xu, X.; Ma, W.; Bo, Z. Fused-Ring Acceptors with Asymmetric Side Chains for High-Performance Thick-Film Organic Solar Cells. *Adv. Mater.* **2017**, *29*, 1703527.
- (9) Meng, H.; Liao, C.; Deng, M.; Xu, X.; Yu, L.; Peng, Q. 18.77 % Efficiency Organic Solar Cells Promoted by Aqueous Solution Processed Cobalt(II) Acetate Hole Transporting Layer. *Angew. Chem., Int. Ed. Engl.* **2021**, *60*, 22554–22561.
- (10) Zhang, J.; Bai, F.; Angunawela, I.; Xu, X.; Luo, S.; Li, C.; Chai, G.; Yu, H.; Chen, Y.; Hu, H.; Ma, Z.; Ade, H.; Yan, H. Alkyl-Chain Branching of Non-Fullerene Acceptors Flanking Conjugated Side

Groups toward Highly Efficient Organic Solar Cells. *Adv. Energy Mater.* **2021**, *11*, 2102596.

(11) Wang, D.; Zhou, G.; Li, Y.; Yan, K.; Zhan, L.; Zhu, H.; Lu, X.; Chen, H.; Li, C. Z. High-Performance Organic Solar Cells from Non-Halogenated Solvents. *Adv. Funct. Mater.* **2021**, *32*, 2107827.

(12) Pan, Y.; Zheng, X.; Guo, J.; Chen, Z.; Li, S.; He, C.; Ye, S.; Xia, X.; Wang, S.; Lu, X.; Zhu, H.; Min, J.; Zuo, L.; Shi, M.; Chen, H. A New End Group on Nonfullerene Acceptors Endows Efficient Organic Solar Cells with Low Energy Losses. *Adv. Funct. Mater.* **2021**, *32*, 2108614.

(13) Li, C.; Zhou, J.; Song, J.; Xu, J.; Zhang, H.; Zhang, X.; Guo, J.; Zhu, L.; Wei, D.; Han, G.; Min, J.; Zhang, Y.; Xie, Z.; Yi, Y.; Yan, H.; Gao, F.; Liu, F.; Sun, Y. Non-Fullerene Acceptors with Branched Side Chains and Improved Molecular Packing to Exceed 18% Efficiency in Organic Solar Cells. *Nat. Energy* **2021**, *6*, 605–613.

(14) Bi, P.; Zhang, S.; Chen, Z.; Xu, Y.; Cui, Y.; Zhang, T.; Ren, J.; Qin, J.; Hong, L.; Hao, X.; Hou, J. Reduced Non-Radiative Charge Recombination Enables Organic Photovoltaic Cell Approaching 19% Efficiency. *Joule* **2021**, *5*, 2408–2419.

(15) Tan, P.; Liu, L.; Chen, Z. Y.; Lai, H.; Zhu, Y.; Chen, H.; Zheng, N.; Zhang, Y.; He, F. Structure–Property Relationships of Precisely Chlorinated Thiophene-Substituted Acceptors. *Adv. Funct. Mater.* **2021**, *31*, 2106524.

(16) Wang, J.; Zheng, Z.; Zu, Y.; Wang, Y.; Liu, X.; Zhang, S.; Zhang, M.; Hou, J. A Tandem Organic Photovoltaic Cell with 19.6% Efficiency Enabled by Light Distribution Control. *Adv. Mater.* **2021**, *33*, No. e2102787.

(17) Bao, S.; Yang, H.; Fan, H.; Zhang, J.; Wei, Z.; Cui, C.; Li, Y. Volatilizable Solid Additive-Assisted Treatment Enables Organic Solar Cells with Efficiency over 18.8% and Fill Factor Exceeding 80%. *Adv. Mater.* **2021**, *33*, 2105301.

(18) Lingxian Meng, Y. Z.; Xiangjian, W.; Chenxi, Li; Xin, Z.; Yanbo, W.; Xin, Ke; Zuo, X.; Liming, D.; Ruoxi, X.; Hin-Lap, Y.; Yong, C.; Yongsheng, C. *Science* **2018**, *361*, 1094–1098.

(19) Chen, Y.; Zheng, Y.; Jiang, Y.; Fan, H.; Zhu, X. Carbon-Bridged 1,2-Bis(2-Thienyl)Ethylene: An Extremely Electron Rich Dithiophene Building Block Enabling Electron Acceptors with Absorption above 1000 Nm for Highly Sensitive Nir Photodetectors. *J. Am. Chem. Soc.* **2021**, *143*, 4281–4289.

(20) Gao, H. H.; Sun, Y.; Cai, Y.; Wan, X.; Meng, L.; Ke, X.; Li, S.; Zhang, Y.; Xia, R.; Zheng, N.; Xie, T.; Li, C.; Zhang, M.; Yip, H. L.; Cao, Y.; Chen, Y. Achieving Both Enhanced Voltage and Current through Fine-Tuning Molecular Backbone and Morphology Control in Organic Solar Cells. *Adv. Energy Mater.* **2019**, *9*, 1901024.

(21) Liu, G.; Li, T.; Zhan, X.; Wu, H.; Cao, Y. High-Sensitivity Visible-near Infrared Organic Photodetectors Based on Non-Fullerene Acceptors. *ACS Appl. Mater. Interfaces* **2020**, *12*, 17769–17775.

(22) Liu, T.; Luo, Z.; Chen, Y.; Yang, T.; Xiao, Y.; Zhang, G.; Ma, R.; Lu, X.; Zhan, C.; Zhang, M.; Yang, C.; Li, Y.; Yao, J.; Yan, H. A Nonfullerene Acceptor with a 1000 Nm Absorption Edge Enables Ternary Organic Solar Cells with Improved Optical and Morphological Properties and Efficiencies over 15%. *Energy Environ. Sci.* **2019**, *12*, 2529–2536.

(23) Wang, D.; Liu, H.; Li, Y.; Zhou, G.; Zhan, L.; Zhu, H.; Lu, X.; Chen, H.; Li, C.-Z. High-Performance and Eco-Friendly Semi-transparent Organic Solar Cells for Greenhouse Applications. *Joule* **2021**, *5*, 945–957.

(24) Wang, W.; Lu, H.; Chen, Z.; Jia, B.; Li, K.; Ma, W.; Zhan, X. High-Performance Nir-Sensitive Fused Tetrathienoacene Electron Acceptors. *J. Mater. Chem. A* **2020**, *8*, 3011–3017.

(25) Yin, H.; Zhang, C.; Hu, H.; Karuthedath, S.; Gao, Y.; Tang, H.; Yan, C.; Cui, L.; Fong, P. W. K.; Zhang, Z.; Gao, Y.; Yang, J.; Xiao, Z.; Ding, L.; Laquai, F.; So, S. K.; Li, G. Highly Crystalline near-Infrared Acceptor Enabling Simultaneous Efficiency and Photostability Boosting in High-Performance Ternary Organic Solar Cells. *ACS Appl. Mater. Interfaces* **2019**, *11*, 48095–48102.

(26) Yin, P.; Yin, Z.; Ma, Y.; Zheng, Q. Improving the Charge Transport of the Ternary Blend Active Layer for Efficient Semi-

- transparent Organic Solar Cells. *Energy Environ. Sci.* **2020**, *13*, 5177–5185.
- (27) Kan, B.; Zhang, J.; Liu, F.; Wan, X.; Li, C.; Ke, X.; Wang, Y.; Feng, H.; Zhang, Y.; Long, G.; Friend, R. H.; Bakulin, A. A.; Chen, Y. Fine-Tuning the Energy Levels of a Nonfullerene Small-Molecule Acceptor to Achieve a High Short-Circuit Current and a Power Conversion Efficiency over 12% in Organic Solar Cells. *Adv. Mater.* **2018**, *30*, 1704904.
- (28) Ma, Y.; Zhang, M.; Wan, S.; Yin, P.; Wang, P.; Cai, D.; Liu, F.; Zheng, Q. Efficient Organic Solar Cells from Molecular Orientation Control of M-Series Acceptors. *Joule* **2021**, *5*, 197–209.
- (29) Xiao, Z.; Liu, F.; Geng, X.; Zhang, J.; Wang, S.; Xie, Y.; Li, Z.; Yang, H.; Yuan, Y.; Ding, L. A Carbon-Oxygen-Bridged Ladder-Type Building Block for Efficient Donor and Acceptor Materials Used in Organic Solar Cells. *Sci. Bull.* **2017**, *62*, 1331–1336.
- (30) An, Q.; Wang, J.; Zhang, F. Ternary Polymer Solar Cells with Alloyed Donor Achieving 14.13% Efficiency and 78.4% Fill Factor. *Nano Energy* **2019**, *60*, 768–774.
- (31) Dai, S.; Zhao, F.; Zhang, Q.; Lau, T.-K.; Li, T.; Liu, K.; Ling, Q.; Wang, C.; Lu, X.; You, W.; Zhan, X. Fused Noncyclic Electron Acceptors for Efficient Polymer Solar Cells. *J. Am. Chem. Soc.* **2017**, *139*, 1336–1343.
- (32) Hou, J.; Inganäs, O.; Friend, R. H.; Gao, F. Organic Solar Cells Based on Non-Fullerene Acceptors. *Nat. Mater.* **2018**, *17*, 119–128.
- (33) Jiao, C.; Guo, Z.; Sun, B.; Yi, Y.-q. -q.; Meng, L.; Wan, X.; Zhang, M.; Zhang, H.; Li, C.; Chen, Y. An Acceptor–Donor–Acceptor Type Non-Fullerene Acceptor with an Asymmetric Backbone for High Performance Organic Solar Cells. *J. Mater. Chem. C* **2020**, *8*, 6293–6298.
- (34) Kan, B.; Feng, H.; Yao, H.; Chang, M.; Wan, X.; Li, C.; Hou, J.; Chen, Y. A Chlorinated Low-Bandgap Small-Molecule Acceptor for Organic Solar Cells with 14.1% Efficiency and Low Energy Loss. *Sci. China Chem.* **2018**, *61*, 1307–1313.
- (35) Ke, X.; Meng, L.; Wan, X.; Cai, Y.; Gao, H.; Yi, Y.; Guo, Z.; Zhang, H.; Li, C.; Chen, Y. A Nonfullerene Acceptor Incorporating a Dithienopyran Fused Backbone for Organic Solar Cells with Efficiency over 14%. *Nano Energy* **2020**, *75*, 104988.
- (36) Lin, Y.; He, Q.; Zhao, F.; Huo, L.; Mai, J.; Lu, X.; Su, C. J.; Li, T.; Wang, J.; Zhu, J.; Sun, Y.; Wang, C.; Zhan, X. A Facile Planar Fused-Ring Electron Acceptor for as-Cast Polymer Solar Cells with 8.71% Efficiency. *J. Am. Chem. Soc.* **2016**, *138*, 2973–2976.
- (37) Luo, Z.; Liu, T.; Xiao, Y.; Yang, T.; Chen, Z.; Zhang, G.; Zhong, C.; Ma, R.; Chen, Y.; Zou, Y.; Lu, X.; Yan, H.; Yang, C. Significantly Improving the Performance of Polymer Solar Cells by the Isomeric Ending-Group Based Small Molecular Acceptors: Insight into the Isomerization. *Nano Energy* **2019**, *66*, 104146.
- (38) Wan, X.; Li, C.; Zhang, M.; Chen, Y. Acceptor-Donor-Acceptor Type Molecules for High Performance Organic Photovoltaics - Chemistry and Mechanism. *Chem. Soc. Rev.* **2020**, *49*, 2828–2842.
- (39) Li, T.; Zhang, H.; Xiao, Z.; Rech, J. J.; Niu, H.; You, W.; Ding, L. A Carbon–Oxygen-Bridged Hexacyclic Ladder-Type Building Block for Low-Bandgap Nonfullerene Acceptors. *Mater. Chem. Front.* **2018**, *2*, 700–703.
- (40) Peng, W.; Zhang, G.; Zhu, M.; Xia, H.; Zhang, Y.; Tan, H.; Liu, Y.; Chi, W.; Peng, Q.; Zhu, W. Simple-Structured Nir-Absorbing Small-Molecule Acceptors with a Thiazolothiazole Core: Multiple Noncovalent Conformational Locks and D-a Effect for Efficient Oscs. *ACS Appl. Mater. Interfaces* **2019**, *11*, 48128–48133.
- (41) Qu, J.; Zhao, Q.; Zhou, J.; Lai, H.; Liu, T.; Li, D.; Chen, W.; Xie, Z.; He, F. Multiple Fused Ring-Based near-Infrared Nonfullerene Acceptors with an Interpenetrated Charge-Transfer Network. *Chem. Mater.* **2019**, *31*, 1664–1671.
- (42) Yao, H.; Cui, Y.; Yu, R.; Gao, B.; Zhang, H.; Hou, J. Design, Synthesis, and Photovoltaic Characterization of a Small Molecular Acceptor with an Ultra-Narrow Band Gap. *Angew. Chem., Int. Ed. Engl.* **2017**, *56*, 3045–3049.
- (43) Zhu, Q.; Liu, D.; Lu, Z.; Gu, C.; Zhang, K.; Bao, X.; Li, Q.; Yang, R. Length Evolution of Fused-Ring Electron Acceptors toward Optimal Blend Morphology in Polymer Solar Cells Incorporating Asymmetric Benzodithiophene-Based Donors. *J. Mater. Chem. A* **2019**, *7*, 4823–4828.
- (44) Zhang, S.; Ma, L.; Ye, L.; Qin, Y.; Xu, Y.; Liu, X.; Wu, Y.; Zhao, W.; Ade, H.; Yao, H.; Hou, J. Modulation of Building Block Size in Conjugated Polymers with D–a Structure for Polymer Solar Cells. *Macromolecules* **2019**, *52*, 7929–7938.
- (45) Song, J.; Li, C.; Ye, L.; Koh, C.; Cai, Y.; Wei, D.; Woo, H. Y.; Sun, Y. Extension of Indacenodithiophene Backbone Conjugation Enables Efficient Asymmetric a–D–a Type Non-Fullerene Acceptors. *J. Mater. Chem. A* **2018**, *6*, 18847–18852.
- (46) Jia, B.; Wang, J.; Wu, Y.; Zhang, M.; Jiang, Y.; Tang, Z.; Russell, T. P.; Zhan, X. Enhancing the Performance of a Fused-Ring Electron Acceptor by Unidirectional Extension. *J. Am. Chem. Soc.* **2019**, *141*, 19023–19031.
- (47) Gao, W.; Liu, T.; Sun, R.; Zhang, G.; Xiao, Y.; Ma, R.; Zhong, C.; Lu, X.; Min, J.; Yan, H.; Yang, C. Dithieno[3,2-B:2',3'-D]Pyrrol-Fused Asymmetrical Electron Acceptors: A Study into the Effects of Nitrogen-Functionalization on Reducing Nonradiative Recombination Loss and Dipole Moment on Morphology. *Adv. Sci.* **2020**, *7*, 1902657.
- (48) Yang, L.; Song, X.; Yu, J.; Wang, H.; Zhang, Z.; Geng, R.; Cao, J.; Baran, D.; Tang, W. Tuning of the Conformation of Asymmetric Nonfullerene Acceptors for Efficient Organic Solar Cells. *J. Mater. Chem. A* **2019**, *7*, 22279–22286.
- (49) Cui, Y.; Yang, C.; Yao, H.; Zhu, J.; Wang, Y.; Jia, G.; Gao, F.; Hou, J. Efficient Semitransparent Organic Solar Cells with Tunable Color Enabled by an Ultralow-Bandgap Nonfullerene Acceptor. *Adv. Mater.* **2017**, *29*, 1703080.
- (50) Gao, H.-H.; Sun, Y.; Wan, X.; Kan, B.; Ke, X.; Zhang, H.; Li, C.; Chen, Y. Design and Synthesis of Low Band Gap Non-Fullerene Acceptors for Organic Solar Cells with Impressively High Jsc over 21 Ma Cm⁻². *Sci. China Mater.* **2017**, *60*, 819–828.
- (51) Zhang, X.; Li, C.; Qin, L.; Chen, H.; Yu, J.; Wei, Y.; Liu, X.; Zhang, J.; Wei, Z.; Gao, F.; Peng, Q.; Huang, H. Side-Chain Engineering for Enhancing the Molecular Rigidity and Photovoltaic Performance of Noncovalently Fused-Ring Electron Acceptors. *Angew. Chem., Int. Ed. Engl.* **2021**, *60*, 17720–17725.
- (52) Ge, G.-Y.; Xiong, W.; Liu, K.-K.; Ryu, H. S.; Wang, S.-S.; Liu, B.; Mahmood, A.; Bai, H.-R.; Wang, J.-F.; Wang, Z.; Woo, H. Y.; Sun, Y.; Wang, J.-L. Synergistic Effect of the Selenophene-Containing Central Core and the Regioisomeric Monochlorinated Terminals on the Molecular Packing, Crystallinity, Film Morphology, and Photovoltaic Performance of Selenophene-Based Nonfullerene Acceptors. *J. Mater. Chem. C* **2021**, *9*, 1923–1935.
- (53) Gao, W.; Fu, H.; Li, Y.; Lin, F.; Sun, R.; Wu, Z.; Wu, X.; Zhong, C.; Min, J.; Luo, J.; Woo, H. Y.; Zhu, Z.; Jen, A. K. Y. Asymmetric Acceptors Enabling Organic Solar Cells to Achieve an over 17% Efficiency: Conformation Effects on Regulating Molecular Properties and Suppressing Nonradiative Energy Loss. *Adv. Energy Mater.* **2020**, *11*, 2003177.
- (54) Li, D.; Sun, C.; Yan, T.; Yuan, J.; Zou, Y. Asymmetric Non-Fullerene Small-Molecule Acceptors toward High-Performance Organic Solar Cells. *ACS Cent. Sci.* **2021**, *7*, 1787–1797.
- (55) Song, X.; Hou, L.; Guo, R.; Wei, Q.; Yang, L.; Jiang, X.; Tu, S.; Zhang, A.; Kan, Z.; Tang, W.; Xing, G.; Müller-Buschbaum, P. Synergistic Interplay between Asymmetric Backbone Conformation, Molecular Aggregation, and Charge-Carrier Dynamics in Fused-Ring Electron Acceptor-Based Bulk Heterojunction Solar Cells. *ACS Appl. Mater. Interfaces* **2021**, *13*, 2961–2970.
- (56) Guo, Q.; Ma, R.; Hu, J.; Wang, Z.; Sun, H.; Dong, X.; Luo, Z.; Liu, T.; Guo, X.; Guo, X.; Yan, H.; Liu, F.; Zhang, M. Over 15% Efficiency Polymer Solar Cells Enabled by Conformation Tuning of Newly Designed Asymmetric Small-Molecule Acceptors. *Adv. Funct. Mater.* **2020**, *30*, 2000383.
- (57) Gao, W.; Liu, T.; Li, J.; Xiao, Y.; Zhang, G.; Chen, Y.; Zhong, C.; Lu, X.; Yan, H.; Yang, C. Simultaneously Increasing Open-Circuit Voltage and Short-Circuit Current to Minimize the Energy Loss in Organic Solar Cells Via Designing Asymmetrical Non-Fullerene Acceptor. *J. Mater. Chem. A* **2019**, *7*, 11053–11061.

(58) Li, X.; Luo, S.; Sun, H.; Sung, H. H.-Y.; Yu, H.; Liu, T.; Xiao, Y.; Bai, F.; Pan, M.; Lu, X.; Williams, I. D.; Guo, X.; Li, Y.; Yan, H. Medium Band-Gap Non-Fullerene Acceptors Based on a Benzothio-phene Donor Moiety Enabling High-Performance Indoor Organic Photovoltaics. *Energy Environ. Sci.* **2021**, *14*, 4555–4563.

(59) Luo, D.; Li, L.; Shi, Y.; Zhang, J.; Wang, K.; Guo, X.; Kyaw, A. K. K. Electron-Deficient Diketone Unit Engineering for Non-Fused Ring Acceptors Enabling over 13% Efficiency in Organic Solar Cells. *J. Mater. Chem. A* **2021**, *9*, 14948–14957.

(60) Liu, S.; Kan, Z.; Thomas, S.; Cruciani, F.; Brédas, J.-L.; Beaujuge, P. M. Thieno[3,4-C]Pyrrole-4,6-Dione-3,4-Difluorothiophene Polymer Acceptors for Efficient All-Polymer Bulk Hetero-junction Solar Cells. *Angew. Chem., Int. Ed. Engl.* **2016**, *55*, 12996–13000.

(61) Gasparini, N.; Salvador, M.; Strohm, S.; Heumueller, T.; Levchuk, I.; Wadsworth, A.; Bannock, J. H.; de Mello, J. C.; Baran, D.; McCulloch, I.; Brabec, C. J.; Brabec, C. J. Burn-in Free Nonfullerene-Based Organic Solar Cells. *Adv. Energy Mater.* **2017**, *7*, 1700770.

(62) Chai, G.; Chang, Y.; Peng, Z.; Jia, Y.; Zou, X.; Yu, D.; Yu, H.; Chen, Y.; Chow, P. C. Y.; Wong, K. S.; Zhang, J.; Ade, H.; Yang, L.; Zhan, C. Enhanced Hindrance from Phenyl Outer Side Chains on Nonfullerene Acceptor Enables Unprecedented Simultaneous Enhancement in Organic Solar Cell Performances with 16.7% Efficiency. *Nano Energy* **2020**, *76*, 105087.

(63) Li, S.; Sun, Y.; Zhou, B.; Fu, Q.; Meng, L.; Yang, Y.; Wang, J.; Yao, Z.; Wan, X.; Chen, Y. Concurrently Improved Jsc, Fill Factor, and Stability in a Ternary Organic Solar Cell Enabled by a C-Shaped Non-Fullerene Acceptor and Its Structurally Similar Third Component. *ACS Appl. Mater. Interfaces* **2021**, *13*, 40766–40777.

(64) Osinsky, A. V.; Bellman, R. A.; Akwani, I. A.; Sachenik, P. A.; Logunov, S. L.; McCamy, J. W. Optical Loss Mechanisms in Gesion Planar Waveguides. *Appl. Phys. Lett.* **2002**, *81*, 2002–2004.

(65) Leong, W. L.; Cowan, S. R.; Heeger, A. J. Differential Resistance Analysis of Charge Carrier Losses in Organic Bulk Heterojunction Solar Cells: Observing the Transition from Bimolecular to Trap-Assisted Recombination and Quantifying the Order of Recombination. *Adv. Energy Mater.* **2011**, *1*, 517–522.

(66) Zhang, X.; Qin, L.; Liu, X.; Zhang, C.; Yu, J.; Xiao, Z.; Zheng, N.; Wang, B.; Wei, Y.; Xie, Z.; Wu, Y.; Wei, Z.; Wang, K.; Gao, F.; Ding, L.; Huang, H. Enhancing the Photovoltaic Performance of Triplet Acceptors Enabled by Side-Chain Engineering. *Solar RRL* **2021**, *5*, 2100522.

Recommended by ACS

Compatibility between Solubility and Enhanced Crystallinity of Benzotriazole-Based Small Molecular Acceptors with Less Bulky Alkyl Chains for Organic Solar Cells

Honggang Chen, Yingping Zou, *et al.*

JULY 22, 2021

ACS APPLIED MATERIALS & INTERFACES

READ 

Microwave-Assisted Synthesis of Non-Fullerene Acceptors and Their Photovoltaic Studies for High-Performance Organic Solar Cells

Sanchari Shome, Hyosung Choi, *et al.*

AUGUST 18, 2021

ACS APPLIED ENERGY MATERIALS

READ 

Tuning of a A–A–D–A–A-Type Small Molecule with Benzodithiophene as a Central Core with Efficient Photovoltaic Properties for Organic Solar Cells

Urwah Azeem, Javed Iqbal, *et al.*

OCTOBER 20, 2021

ACS OMEGA

READ 

Cardanol- and Guaiacol-Sourced Solution-Processable Green Small Molecule-Based Organic Solar Cells

Barla Rajkumar, Bimlesh Lochab, *et al.*

MARCH 30, 2020

ACS SUSTAINABLE CHEMISTRY & ENGINEERING

READ 

Get More Suggestions >